

# 多层激光熔覆对 30CrMnSiNi2A 高强钢组织与性能的影响

庞小通<sup>1</sup>, 姚成武<sup>1\*</sup>, 龚群甫<sup>2</sup>, 王志杰<sup>2</sup>, 李铸国<sup>1</sup>

<sup>1</sup> 上海交通大学材料科学与工程学院上海市激光制造与材料改性重点实验室, 上海 200240;

<sup>2</sup> 中国人民解放军第四七二四工厂, 上海 200436

**摘要** 在 30CrMnSiNi2A 高强钢基体上进行多层激光熔覆, 研究各层熔覆热循环对基体组织与力学性能的影响。结果表明: 在组织方面, 熔覆盖面层时均对基体重新淬硬, 由于已沉积熔覆层会吸收激光热量, 故基体淬硬深度会随着层数的增加而逐渐减小, 淬硬深度减小至对基体不能完全奥氏体化时, 出现了不完全淬硬现象; 继续增加熔覆层数, 熔覆层不再重新淬硬基体, 产生了回火作用。多层熔覆时每一层均对基体有回火作用, 随着层数的增加, 基体马氏体板条束间残余奥氏体首先分解, 接着碳化物逐渐析出, 马氏体板条粗化变宽、块状化, 直至板条状马氏体特征消失, 完全转变为索氏体组织。在力学性能方面, 随着层数增加, 基体热影响区试样变化趋势为抗拉强度逐渐降低、冲击韧性逐渐升高。由于激光快速加热, 首层熔覆对基体回火残余奥氏体分解不明显, 次层或后续层熔覆对基体残余奥氏体产生明显的分解作用, 故残余奥氏体相减少, 造成拉伸延伸率、冲击韧性均略有降低。随着熔覆层数增加, 基体热影响区拉伸延伸率增加, 拉伸断裂沿高温回火区启裂、扩展; 熔覆层数继续增加, 直至对基体产生不完全淬火时, 拉伸断裂可分别在不完全淬火区、高温回火区多点启裂、扩展, 拉伸塑性变形协调性下降, 造成基体热影响区试样延伸率显著下降。

**关键词** 激光技术; 激光熔覆; 热循环; 热影响区; 微观组织; 力学性能

中图分类号 V261.8 文献标志码 A

doi: 10.3788/CJL202148.0602104

## 1 引言

与常规焊接修复方法相比, 激光熔覆作为一种先进表面改性技术, 利用熔覆过程中非平衡加工条件(快速加热和冷却), 在高强钢构件表面熔覆同种成分或近似成分的铁基涂层材料, 可获得晶粒细化、高位错密度的修复层, 从而实现修复层高强度、高韧性的力学性能, 因此在高强钢构件表面修复上具有潜在的优势<sup>[1-3]</sup>。近年来针对高强钢的激光熔覆修复有较多报道<sup>[4-12]</sup>, 如 Sun 等<sup>[4]</sup>采用质量分数为 0.4% 的 AISI 4340 合金粉末和质量分数为 0.25% 的 AerMet 100 粉末, 修复 AISI4340 钢, 低碳含量的熔覆材料有利于提升熔覆试样的拉伸性能和疲劳性能; Liu 等<sup>[7]</sup>在 300M 基板上激光熔覆 AerMet100 粉末, 可获得较好的拉伸性能。

采用传统焊接方法进行高强钢多层多道补焊修复, 其中多次焊接热循环使得热影响区(HAZ)晶粒粗大, 引起材料性能脆化, 显著降低了钢基体的冲击韧性<sup>[13-17]</sup>。与传统焊接类似, 激光熔覆中多层多道热循环会对基体的淬硬区产生多次回火作用<sup>[18-19]</sup>, 从而使得基体热影响区出现晶粒粗化、软化现象, 显著降低了高强钢修复件基体的力学性能<sup>[4-5]</sup>。文献中针对多层多道激光熔覆中基体热影响区对性能的影响有较多报道。Rashid 等<sup>[6]</sup>在 300M 基板上多层多道熔覆质量分数为 0.3% 的 300M 合金粉, 熔覆层和热影响区中回火马氏体相和未回火马氏体相分布不均匀, 导致试样拉伸各向异性; 针对高强钢基体热影响区性能下降的问题, Sun 等<sup>[5]</sup>通过在激光多层多道熔覆中利用间歇时间控制热输入量, 在熔覆层和热影响区采用部分回火的方式, 提高了试样屈服强

收稿日期: 2020-07-01; 修回日期: 2020-08-03; 录用日期: 2020-08-21

基金项目: 上海市军民融合专项(JMRH-2018-1033)

\*E-mail: yaochwu@sjtu.edu.cn

度和韧性;针对激光熔覆热循环对FV520B马氏体不锈钢基体组织的影响,Xu等<sup>[20]</sup>通过热模拟试验得出热循环最高温度决定热影响区组织演变的结论,推测可知降低扫描速度可以控制热影响区的冲击韧性,减小延伸率的下降量。目前,对于多层多道修复高强度钢构件,不仅需有效调控熔覆层的组织和性能,还需克服基体热影响区软化而导致力学性能劣化问题<sup>[4]</sup>,因此研究多重热循环对基体热影响区组织演化(淬硬和回火等)和力学性能变化趋势,有利于对修复件强韧性的调控。但目前揭示其规律和作用机制的研究甚少,不利于高强钢激光修复工艺方案的制定。

鉴于上述情况,本文以重要受力结构部件(如高强度连接件和轴类零件等)用钢30CrMnSiNi2A为激光熔覆修复的研究对象,在其表面实施1层~8层的多层连续激光熔覆,研究各熔覆层多次热循

环对基体热影响区组织和性能的影响。本文研究可为类似30CrMnSiNi2A高强钢修复方案提供理论依据和参考。

## 2 实验材料和方法

实验用的合金粉末为30CrMnSiA粉末(质量分数:0.286% C,0.954% Cr,1.012% Mn,0.977% Si),球形粉末平均粒径为118 μm。实验用的基板为30CrMnSiNi2A钢(质量分数:0.296% C,0.965% Cr,1.124% Mn,0.982% Si,1.532% Ni),尺寸为120 mm×60 mm×10 mm,其微观组织如图1所示,主要为板条马氏体和弥散析出的碳化物质点。在进行实验之前,基板表面经SiC砂纸打磨后,用丙酮清洗、干燥,除去污染物,粉末在真空干燥箱中烘干处理3 h,温度为85 °C。

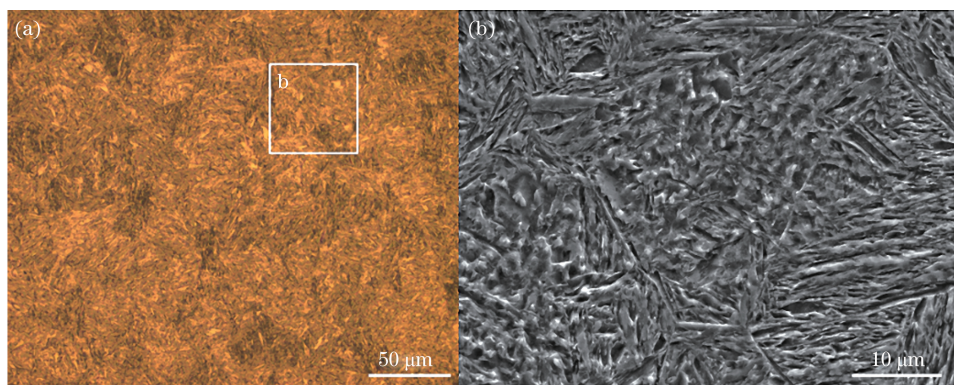


图1 30CrMnSiNi2A钢基体。(a)金相组织;(b)图1(a)中的局部放大

Fig. 1 30CrMnSiNi2A substrate. (a) Metallographic microstructure; (b) local magnification in Fig. 1(a)

实验用的激光器为Laserline LDF-8000-60型高功率激光器,其最大功率为8 kW,光斑尺寸为φ7.3 mm,采用同轴送粉形式,熔覆过程在高纯Ar气保护下进行,装置如图2(a)所示。使用优化的多

层多道工艺参数进行单道多层试验:激光功率为2.1 kW,扫描速度为9 mm/s,送粉速度10 g/min,送粉气流量为10 L/min,保护气为20 L/min。单层熔覆厚度为0.3 mm,分别激光熔覆单道1~8层

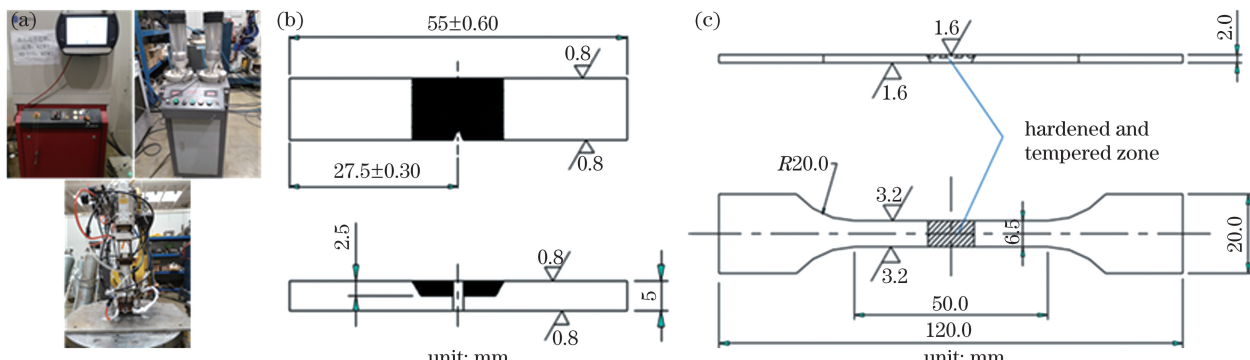


图2 激光熔覆和30CrMnSiNi2A钢激光淬硬和回火力学试样加工尺寸图。(a)激光熔覆装置;(b)冲击试样;

Fig. 2 Photographs of required equipment for laser cladding and the geometric shapes and sizes of mechanical specimens for 30CrMnSiNi2A steel in laser quenching and tempering states. (a) Equipment for laser cladding; (b) impact specimens; (c) tensile specimens

涂层,试样空冷至室温。

垂直于熔覆方向,切割出尺寸为 $10\text{ mm} \times 10\text{ mm} \times 10\text{ mm}$ 的金相试样,砂纸打磨后经机械抛光、腐蚀(腐蚀试剂采用体积分数为4%的硝酸乙醇)。微观组织采用Zeiss-AxioCam MRc5光学显微镜(OM)和TESCAN-LYRA3扫描电子显微镜(SEM)表征。显微硬度采用Zwick/Roell ZH $\mu$ 维氏显微硬度计表征。测试载荷为0.5 kgf(1 kgf = 9.8 N),保载时间为15 s,压痕间距为400  $\mu\text{m}$ ,测试三行,取其平均值。图2(b)和图2(c)为拉伸试样和冲击试样加工尺寸图,切削掉熔覆涂层,保留激光热循环对基体的淬硬层和回火区,在Zwick/Roell Z100拉伸试验机和300 J冲击试验机上进行拉伸性能测试。

### 3 分析与讨论

#### 3.1 宏观与微观组织

图3为30CrMnSiNi2A基体上分别熔覆1~8层涂层横截面宏观形貌,其中呈月牙形的亮区为激光热循环产生的淬硬层。激光熔覆热循环对

30CrMnSiNi2A钢基体产生淬硬,在多层激光熔覆中,每层均会对基体产生淬硬,且后层会对前层基体淬硬区重新淬硬,熔覆层数越多,基体淬硬次数就越多。图3(a)~图3(f)所示的1~6层熔覆,随着熔覆层数的增加,30CrMnSiNi2A钢基体月牙形淬硬层深度逐渐降低,具体淬硬层深度数据见表1。月牙形轮廓为最后层淬硬层的形状,由图3可见,后层淬硬区面积小于前层基体淬硬区,这表明后层并不能重新淬硬整个前层淬硬区,但其热循环会对前层淬硬层产生回火分解而使前层月牙形轮廓消失。至第7层后,激光熔覆层对基体不再完全淬硬,基体激光淬硬层仍保留第6层淬硬层月牙形轮廓,见图3(g)~图3(h)所示。

为了区分多层熔覆下激光热循环对基体组织的影响,将30CrMnSiNi2A钢基体激光热影响区分为激光淬硬区、高温回火区和一般回火区,其中高温回火区为激光淬硬区附近区域,一般回火区位于距熔合线2.0 mm处,具体分别见图3(a)的A1、B1、C1所示位置。

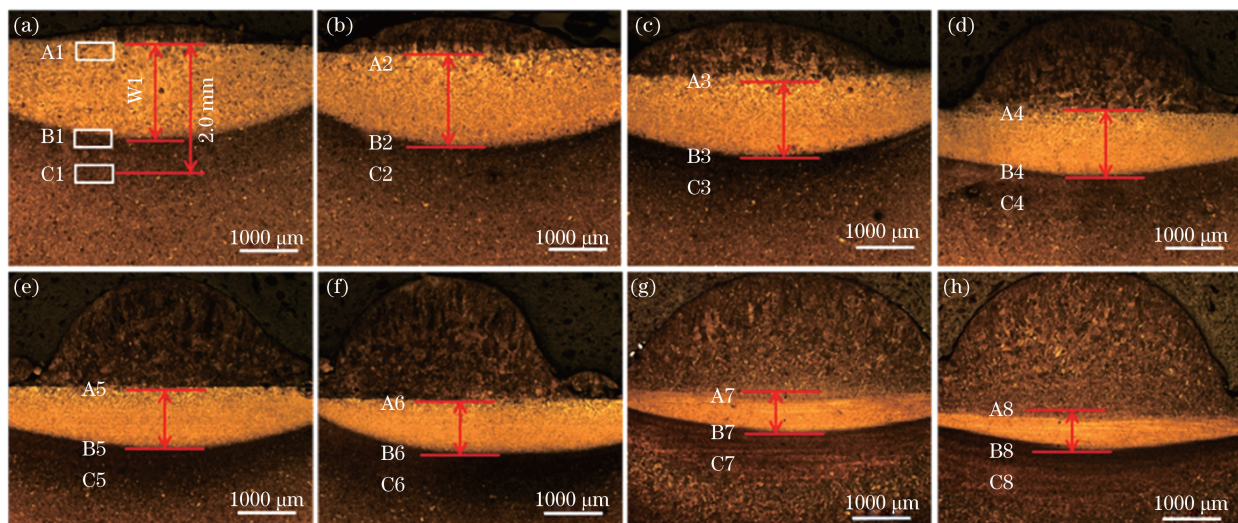


图3 30CrMnSiNi2A基体上多层熔覆30CrMnSiA涂层试样的横截面宏观形貌。(a)熔覆1层;(b)熔覆2层;(c)熔覆3层;(d)熔覆4层;(e)熔覆5层;(f)熔覆6层;(g)熔覆7层;(h)熔覆8层

Fig. 3 Macroscopic morphology in the cross section of 30CrMnSiNi2A substrates under multiple cladding 30CrMnSiA coating. (a) 1 layer; (b) 2 layers; (c) 3 layers; (d) 4 layers; (e) 5 layers; (f) 6 layers; (g) 7 layers; (e) 8 layers

表1 多层熔覆30CrMnSiNi2A基体时的激光淬硬深度

Table 1 Quenching depth of 30CrMnSiNi2A substrate by multiple laser cladding

Cladding layer	1	2	3	4	5	6	7	8
Quenching depth /mm	1.61	1.40	1.24	1.05	0.91	0.77	0.75	0.75

图4为30CrMnSiNi2A基体激光淬硬层微观组织,位于图3中各涂层的A1~A8区域,图4(a)~图4(h)均为多层激光熔覆的基体淬硬组织。如

图4(a)~图4(f)所示,在熔覆1~6层中,随着层数增加,前道涂层会吸收热量,激光热循环对基体的影响会减小,盖面层对基体的热影响减弱,基体表层区

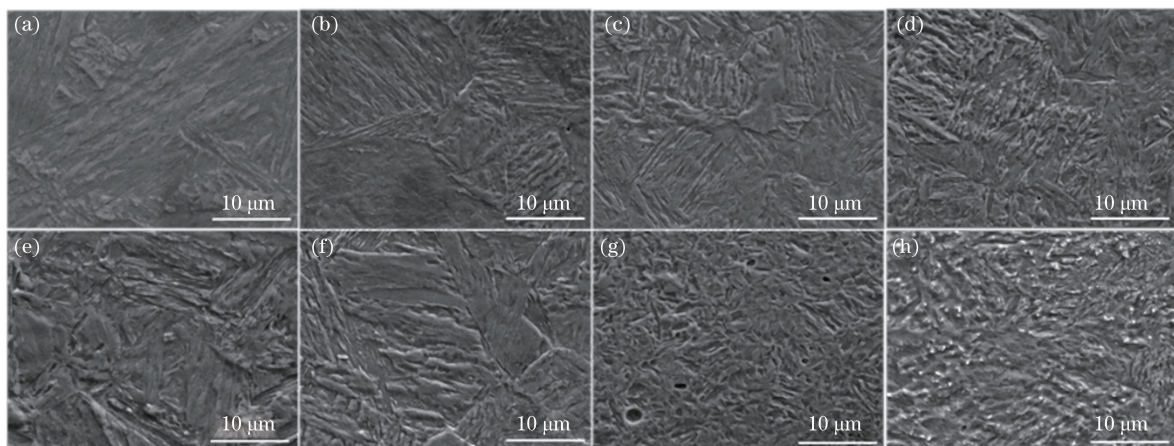


图 4 30CrMnSiNi2A 基体激光淬火区的淬硬组织(位于图 3)。(a)熔覆 1 层, A1 区;(b)熔覆 2 层, A2 区;(c)熔覆 3 层, A3 区;(d)熔覆 4 层, A4 区;(e)熔覆 5 层, A5 区;(f)熔覆 6 层, A6 区;(g)熔覆 7 层, A7 区;(h)熔覆 8 层, A8 区

Fig. 4 Microstructures of laser quenching zone in the 30CrMnSiNi2A substrate (located in Fig. 3). (a) 1 layer, A1 zone; (b) 2 layers, A2 zone; (c) 3 layers, A3 zone; (d) 4 layers, A4 zone; (e) 5 layers, A5 zone; (f) 6 layers, A6 zone; (g) 7 layers, A7 zone; (h) 8 layers, A8 zone

重新奥氏体化的温度降低,造成基体淬硬层深度减小;在多层激光熔覆过程中,热量将通过前熔覆层热传导传输至基体表层区,致使该区发生奥氏体相变,在随后的快速冷却过程中奥氏体将转变为细小板条状马氏体组织。随着熔覆层数的增加,由于热传导传输至基体表面的热量降低,淬火硬化区面积减少。当熔覆至第 7 层时,基体表面温度降至  $A_{c1} \sim A_{c3}$  之间( $A_{c1}$ :加热时珠光体向奥氏体转变的开始温度; $A_{c3}$ :加热时先共析铁素体全部转变为奥氏体的终止温度),致使先前马氏体向奥氏体的转变以及碳的溶解不能充分进行,出现了不完全淬硬现象<sup>[21]</sup>。当熔覆至第 8 层时,回火索氏体形成。

图 5 为 30CrMnSiNi2A 基体激光高温回火区微

观组织。由图 5 可见,当熔覆前两层时,基体回火区组织仍保持马氏体的形态特征,在熔覆第 2 层时马氏体板条束腐蚀变深,这可能是马氏体板条束间的残余奥氏体薄膜分解降低了其耐腐蚀性所致。但随着熔覆层数逐渐增加,回火区组织开始有回火索氏体形成,且其分数呈现出逐渐增多的变化趋势。在熔覆第 8 层时,甚至可以获得完全回火索氏体组织。上述组织的演化规律主要与 Si 在铁中具有高的扩散激活能有关<sup>[22-23]</sup>。在前两层的熔覆过程中,由于热作用时间较短,扩散较慢的 Si 抑制了碳化物的析出,在很大程度上阻碍了回火马氏体分解。而随着熔覆层数的增加,由于多次循环热作用有利于 Si 的充分扩散,回火区组织逐渐由回火马氏体向回火索氏体演化。

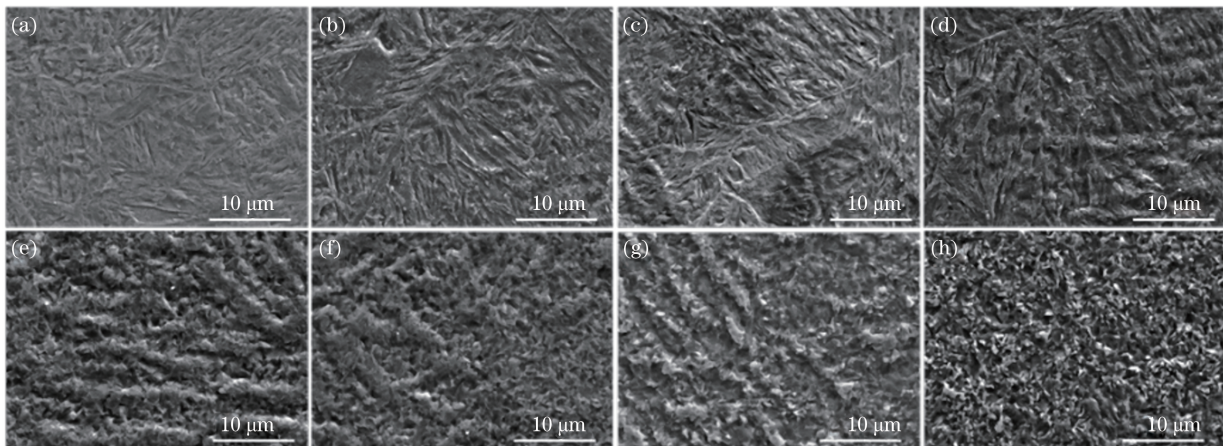


图 5 30CrMnSiNi2A 基体激光高温回火区微观组织(位于图 3)。(a) B1 区;(b) B2 区;(c) B3 区;(d) B4 区;(e) B5 区;(f) B6 区;(g) B7 区;(h) B8 区

Fig. 5 Microstructures of high temperature tempering zone in the 30CrMnSiNi2A substrate (located in Fig. 3). (a) B1 zone; (b) B2 zone; (c) B3 zone; (d) B4 zone; (e) B5 zone; (f) B6 zone; (e) B7 zone; (e) B8 zone

图6为30CrMnSiNi2A基体一般回火区微观组织,位于图3中各涂层的C1~C8处。熔覆1层后,由于激光热循环快速回火时间极短,一般回火区温度较低,基体马氏体组织几乎没有变化,如图6(a)所示。在熔覆2~5层后,分别经历2~5次激光热循环后,基体马氏体回火程度增加,马氏体板条束间碳化物析出增加,但马氏体板条长度几乎没有

变化,见图6(b)~图6(e)所示。熔覆6层后,基体马氏体长板条束回火溶解成短棒状,马氏体转变成索氏体的体积分数大幅增加,如图6(f)所示。在熔覆7层后,基体以索氏体为主,含有少量回火马氏体组织,如图6(g)所示。熔覆8层后,在8次激光热循环作用下,基体马氏体组织完全回火分解成索氏体组织,如图6(h)所示。

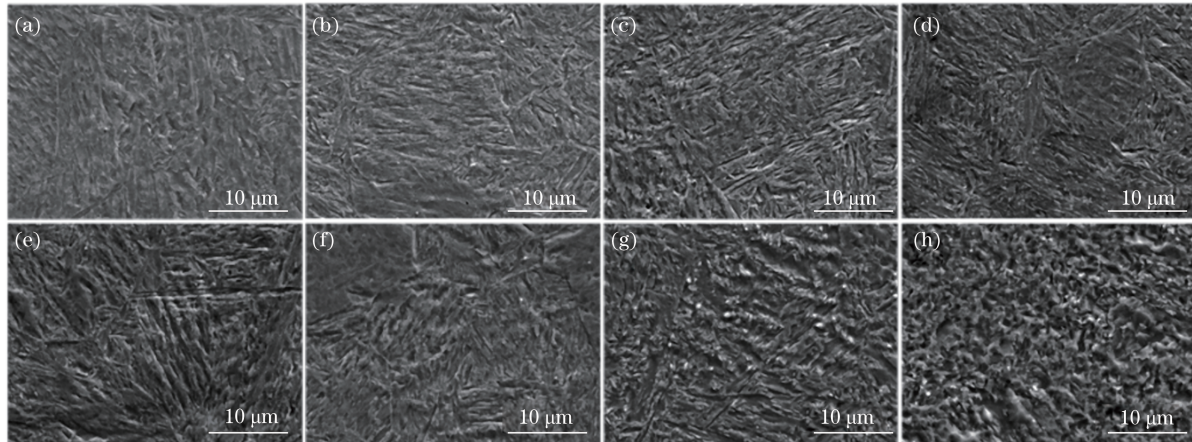


图6 30CrMnSiNi2A基体激光一般回火区微观组织(位于图3中各涂层的C1~C8处)。(a) C1区;(b) C2区;(c) C3区;(d) C4区;(e) C5区;(f) C6区;(g) C7区;(h) C8区

Fig. 6 Microstructures of partial tempering zone in the 30CrMnSiNi2A substrate (located at C1-C2 of each coating in Fig. 3).

(a) C1 zone; (b) C2 zone; (c) C3 zone; (d) C4 zone; (e) C5 zone; (f) C6 zone; (g) C7 zone; (h) C8 zone

### 3.2 力学性能

30CrMnSiNi2A钢为马氏体组织,基体硬度为550 HV~600 HV。表2列出30CrMnSiNi2A基体经多层熔覆的激光热影响区硬度值。激光热影响区

存在淬硬区和回火软化区,其中激光淬硬层的硬度为610 HV~660 HV,回火软化区的硬度为400 HV~530 HV。由表2可见,随着激光熔覆层数的增加,基体热影响区的平均硬度逐渐下降。

表2 30CrMnSiNi2A基体激光热影响区硬度值

Table 2 Hardness values of 30CrMnSiNi2A substrate in heat-affected zone

Cladding layer		1	2	3	4	5	6	7	8
Hardness / (HV <sub>0.5 kgf</sub> )	Quenching zone	643.3	640.5	634.4	636.1	611.2	583.8	576.7	598.5
		624.2	646.0	657.5	657.4	626.0	636.1	643.2	635.7
		629.6	611.2	624.5	629.6	433.5	436.6	428.6	430.9
		488.6	457.5	459.2	446.1	446.1	430.4	452.6	459.2
		454.2	467.7	447.1	435.6	452.6	456.2	447.7	411.3
	Tempering zone	530.2	487.2	469.4	467.7	462.6	474.3	464.6	417.1
		569.7	560.5	540.7	511.9	516.3	506.1	481.8	511.9
	Substrate	567.4	567.4	567.4	560.5	556.0	538.6	524.0	528.1
		581.4	588.6	576.7	576.7	583.8	565.1	574.3	569.7
		596.0	601.0	598.5	586.2	591.1	588.6	591.1	583.8
Average of hardness in HAZ / (HV <sub>0.5 kgf</sub> )		561.7	551.7	548.9	540.6	506.9	503.4	502.4	499.1

图7为30CrMnSiNi2A基体激光热影响区的拉伸性能曲线。除了多层熔覆2层和7层,基体激

光热影响区拉伸性能的趋势为:随着熔覆层数增加,抗拉强度下降,按升序排序为8层、6层、5层、7层、

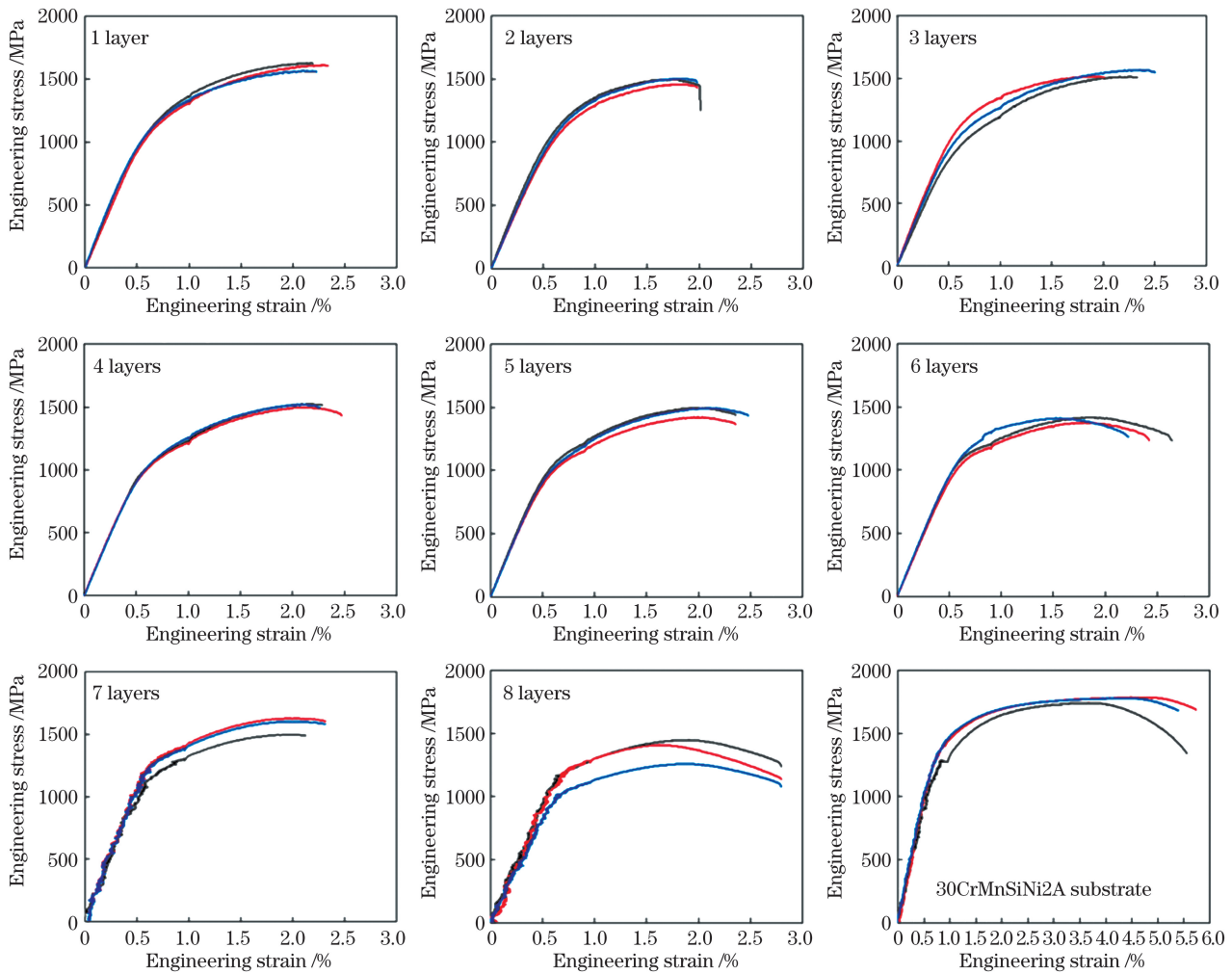


图 7 30CrMnSiNi2A 基体热影响区(1层~8层熔覆)和30CrMnSiNi2A母材的拉伸性能曲线

Fig. 7 Tensile properties of 30CrMnSiNi2A substrate with HAZ (1 layer to 8 layers) and 30CrMnSiNi2A substrate

4层、3层、2层、1层,由1600 MPa下降至1400 MPa。随着熔覆层数的增加,基体热影响区的强度持续下降,但延伸率有所升高,由2.1%上升至2.9%;与30CrMnSiNi2A母材性能相比,在激光熔覆热循环作用下,基体热影响区的强度和塑性延伸率均降低,其中抗拉强度下降至母材的78%~88%,延伸率下降至母材的37%~49%。

尽管激光熔覆热循环降低了基体的延伸率,但不同层数的熔覆层对30CrMnSiNi2A基体的多次淬火和回火,导致基体热影响区延伸率存在拐点,其延伸率值按升序排序为:2层、7层、1层、3层、4层、5层、6层、8层,即总趋势为随着熔覆层数增加,基体热影响区延伸率增加,但其中出现突变点,即熔覆2层和熔覆7层时的基体热影响区。

图8为多层熔覆后30CrMnSiNi2A基体热影响区试样拉伸断裂位置,多次激光热循环作用的基体热影响区断裂启裂点为:熔覆1~5层,裂纹启裂

点为激光高温回火区,随着层数增加,马氏体组织粗化程度增加,见图8(a)~图8(e)所示;熔覆6层,裂纹启裂点有2处,分别为激光高温回火区(其马氏体组织已部分分解成索氏体)和一般回火区(其马氏体组织已完全分解成索氏体),见图8(f)所示;熔覆7层,裂纹启裂点也为2处,分别为激光不完全淬硬区(不完全淬硬马氏体组织)和前道次第6层的激光淬硬层高温回火区,见图8(g)所示;熔覆8层,裂纹启裂点为前道第7层熔覆的基体淬硬层高温回火区。30CrMnSiNi2A钢中碳含量较低,完全淬硬产生的位错马氏体强度较高,且具有一定的韧性,而高温回火区硬度值较低,因此在拉伸应力作用下,高温回火区会首先出现塑性变形不协调导致的应力集中现象,裂纹源主要在高温回火区形核生长。

图9为30CrMnSiNi2A基体热影响区拉伸试样断裂形貌。熔覆1层、2层后,基体热影响区断

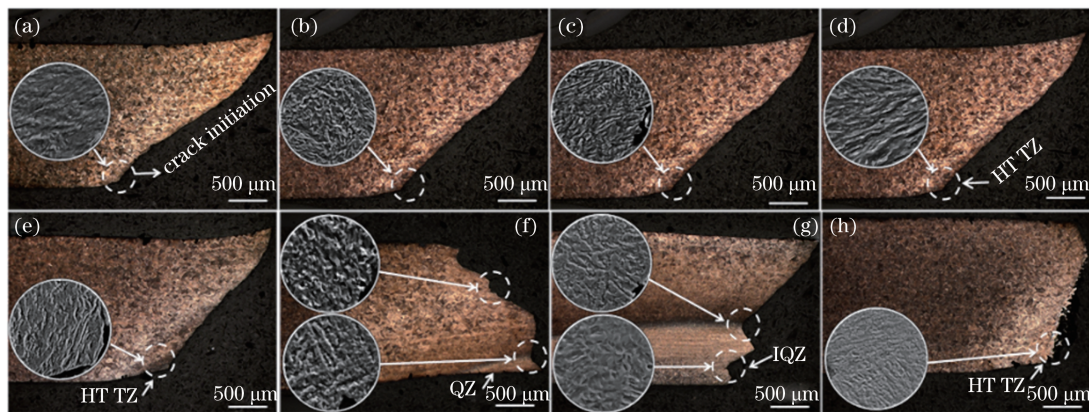


图 8 30CrMnSiNi2A 基体热影响区拉伸试样断裂启裂端。(a)熔覆 1 层的高温回火区;(b)熔覆 2 层的高温回火区;(c)熔覆 3 层的高温回火区;(d)熔覆 4 层的高温回火区;(e)熔覆 5 层的高温回火区;(f)熔覆 6 层的激光高温回火区+一般回火区;(g)熔覆 7 层的激光淬硬区+第 6 层激光淬硬层的高温回火区;(h)熔覆 8 层,第 7 层淬硬层的高温回火区

Fig. 8 Initiation fracture position of tensile specimens in HAZ of the 30CrMnSiNi2A substrate. (a) High temperature tempering zone (HTTZ) in 1 cladding layer; (b) HTTZ in 2 cladding layers; (c) HTTZ in 3 cladding layers; (d) HTTZ in 4 cladding layers; (e) HTTZ in 5 cladding layers; (f) HTTZ in 6 cladding layers+partial tempering zone (TZ); (g) incomplete quenching zone (IQZ) in 7 cladding layers+HTTZ in 6th-cladding layer; (h) HTTZ of 7th-cladding layer in 8 cladding layers

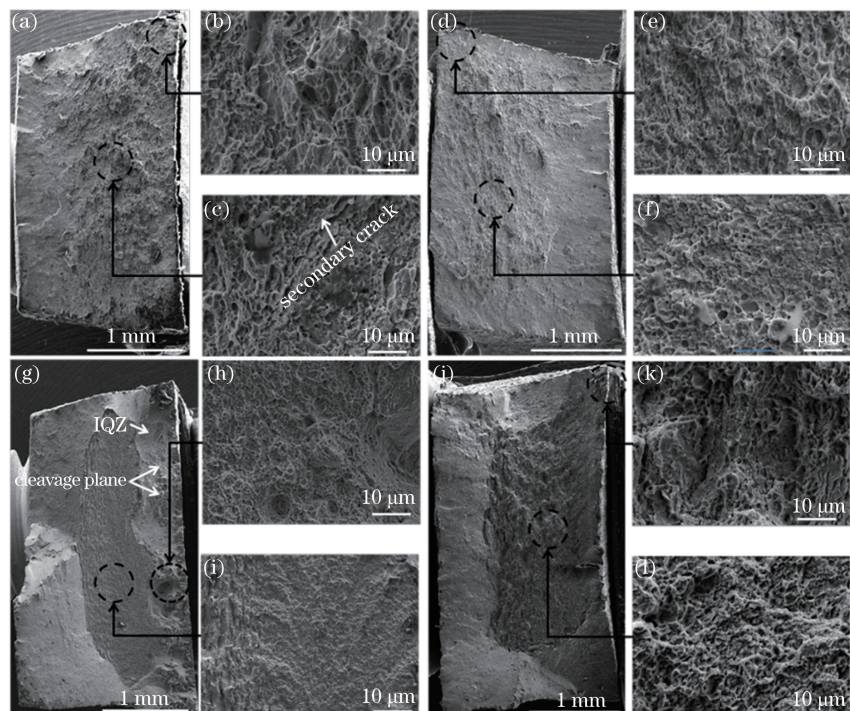


图 9 多层激光熔覆后的 30CrMnSiNi2A 基体热影响区拉伸试样断口形貌。(a)~(c)熔覆 1 层的断口宏观形貌及其裂纹源区和裂纹扩展区;(d)~(f)熔覆 2 层的断口宏观形貌及其裂纹源区和裂纹扩展区;(g)~(i)熔覆 7 层的断口宏观形貌及其裂纹源区和裂纹扩展区;(j)~(l)熔覆 8 层的断口宏观形貌及其裂纹源区和裂纹扩展区

Fig. 9 Fracture morphology of the tensile specimens of the 30CrMnSiNi2A substrate with HAZ after multiple layer cladding. (a) Macro-morphology of the fracture for 1 cladding layer; (b) crack initiation zone and (c) crack growth zone are shown in Fig. 9(a); (d) macro-morphology of the fracture for 2 cladding layers; (e) crack initiation zone and (f) crack growth zone are shown in Fig. 9(d); (g) macro-morphology of the fracture for 7 cladding layers; (h) crack initiation zone and (i) crack growth zone are shown in Fig. 9 (g); (j) macro-morphology of the fracture for 8 cladding layers; (k) crack initiation zone and (l) crack growth zone are shown in Fig. 9(j)

口宏观形貌分布见图9(a)、图9(d),区别在于熔覆1层的裂纹源区韧窝尺寸、深度均大于熔覆2层,分别见图9(b)、图9(e);熔覆1层的裂纹扩展区存在浅的二次裂纹,而熔覆2层的裂纹扩展区未见二次裂纹,分别见图9(c)、图9(f)。这些断口形貌的差异,表现为熔覆1层的基体热影响区抗拉强度和延伸率均高于熔覆2层,其原因可能为30CrMnSiNi2A基体中马氏体板条间分布有残余奥氏体薄膜。在激光熔覆2层后,经2次激光熔覆层的高温回火,其基体高温回火区马氏体板条间残余奥氏体的分解更充分,马氏体板条较熔覆1层的更易腐蚀[见图5(a)、图5(b)],这是因为残余奥氏体分解,而马氏体板条并未分解,降低了热影响区的韧性。

熔覆7层的30CrMnSiNi2A基体热影响区试样拉伸断口宏观形貌见图9(g),裂纹源区在激光不完全淬硬区时,裂纹分别在不完全淬硬区和回火区扩展,在不完全淬硬区存在局部断裂解理面[如图9(g)箭头所示],且断口瞬断区(剪切唇)面积比较大。裂纹源区为高温回火区时,韧窝较深、塑韧性较高,如图9(h)所示,其原因为该区马氏体已大量回火分解成索氏体,提高了局部韧性[见图5(g)]。对应的裂纹扩展区位于激光热影响区的一般回火区,图9(i)给出

裂纹扩展区韧窝形貌,韧窝深度大于熔覆1层、熔覆2层的裂纹扩展区,对比图6(a)、图6(b)、图6(g),可知其原因为熔覆7层的基体一般回火区大量马氏体分解成索氏体,提高了塑性。由此可见,熔覆7层的基体热影响区高温回火区、一般回火区塑性均高于熔覆1层、熔覆2层试样,然而熔覆7层试样的拉伸延伸率差,这可能是因为熔覆7层的基体存在不完全淬火区,该区硬度下降(见表2所示),强度降低,使得拉伸断裂可在不完全淬火区形成多点裂纹源,在该区、高温回火区同时进行裂纹扩展[见图9(g)、图8(g)],且由于不完全淬火区和高温回火区组织性能不均匀性差异大,其变形协调能力变差,难以均匀变形所致。

熔覆8层的30CrMnSiNi2A基体热影响区试样拉伸断口宏观形貌见图9(j)。其裂纹源区在高温回火区,其韧窝尺寸较大、韧窝较深,如图9(k)所示。其裂纹扩展区均匀,韧窝明显更深,如图9(l)所示。强塑积(用抗拉强度与延伸率的乘积表示)可用来表征高强钢的强度和塑性的平衡<sup>[24-27]</sup>。表3为30CrMnSiNi2A基体和基体热影响区的强塑积,由此可见,熔覆8层的30CrMnSiNi2A基体热影响区具有最优的塑韧性,具体表现为基体热影响区拉伸试样延伸率最高。

表3 30CrMnSiNi2A基体和基体热影响区的强塑积

Table 3 Product of strength and elongation (PSE) of 30CrMnSiNi2A substrates and substrates with different HAZs

Cladding layer	0	1	2	3	4	5	6	7	8
Tensile strength / MPa	1767	1602	1531	1528	1512	1488	1461	1498	1427
Elongation / %	5.56	2.25	2.10	2.27	2.32	2.35	2.44	2.24	2.85
PSE / (MPa · %)	9824.5	3604.5	3215.1	3468.5	3507.8	3496.8	3564.8	3355.5	4066.9

图10为30CrMnSiNi2A基体激光热影响区试样的室温冲击韧性,随着熔覆层数的增加,基体热影

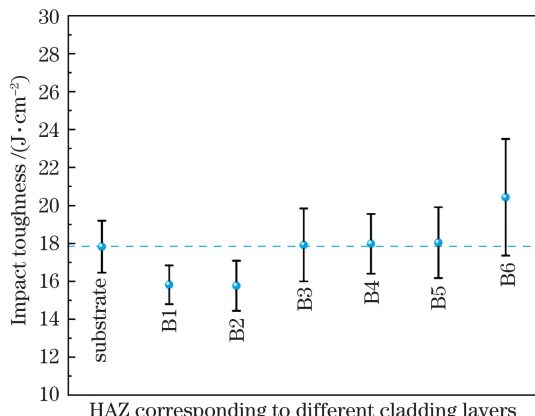


图10 30CrMnSiNi2A基体激光热影响区的冲击韧性

Fig. 10 Impact toughness of HAZ in 30CrMnSiNi2A substrate according to different cladding layers

响区的冲击韧性逐渐增加,且超过基体的冲击韧性。其中,相比较熔覆1层,熔覆2层和3层基体热影响区冲击韧性略有下降,这是因为基体高温回火区更多马氏体板条形态未发生变化,而板条束间奥氏体大量分解所致。

## 4 结 论

在30CrMnSiNi2A高强钢表面分别进行1~8层的多层熔覆试验,研究激光熔覆热循环对基材组织和力学性能的影响,可得以下结论:

- 1) 激光熔覆每一层后均对高强钢基体重新淬硬。淬硬过程中由于前道熔覆层会吸收激光热量,基体淬硬深度会随着层数增加而逐渐减小,淬硬深度减小至对基体不能完全奥氏体化时,出现了不完全淬硬现象;熔覆层数增加至8层以后,熔覆层将不

再重新淬硬基体,而是产生了回火作用。

2) 激光熔覆每一层后均对高强钢基体产生回火作用,随着层数的增加,高强钢基体马氏体板条束间残余奥氏体首先分解,接着碳化物逐渐析出,马氏体板条粗化变宽、块状化,直至板条状马氏体特征消失,高强钢基体回火区完全转变为索氏体组织。

3) 随着层数增加,基体热影响区试样变化趋势为抗拉强度逐渐降低、冲击韧性逐渐升高。由于激光加热速度快,首层熔覆对基体回火残余奥氏体分解不明显,次层熔覆会对基体残余奥氏体产生明显分解作用,故韧性残余奥氏体相减少,造成2层熔覆的拉伸延伸率、冲击韧性均略有降低。

4) 随着熔覆层数增加,基体热影响区拉伸延伸率增加,由2.1%上升至2.9%,拉伸断裂沿高温回火区启裂、扩展;但熔覆至第7层时,激光熔覆热循环对高强钢基体产生不完全淬火,拉伸断裂分别在不完全淬火区、高温回火区多点启裂、扩展,拉伸塑性变形协调性下降,造成拉伸试样延伸率显著下降。

## 参 考 文 献

- [1] Toyserkani E, Khajepour A, Corbin S F. Laser cladding[M]. Boca Raton: CRC Press, 2004.
- [2] Wan X R, Xu C G. High strength and ultra-high strength steel [M]. Beijing: China Machine Press, 1988.  
万翛如, 许昌淦. 高强度及超高强度钢[M]. 北京: 机械工业出版社, 1988.
- [3] Wang H M. Research progress on laser surface modifications of metallic materials and laser rapid forming of high performance metallic components [J]. Acta Aeronautica et Astronautica Sinica, 2002, 23(5): 473-478.  
王华明. 金属材料激光表面改性与高性能金属零件激光快速成形技术研究进展[J]. 航空学报, 2002, 23(5): 473-478.
- [4] Sun S D, Liu Q C, Brandt M, et al. Effect of laser clad repair on the fatigue behaviour of ultra-high strength AISI 4340 steel [J]. Materials Science and Engineering: A, 2014, 606: 46-57.
- [5] Sun S D, Liu Q C, Barr C, et al. In-situ quench and tempering for microstructure control and enhanced mechanical properties of laser cladded AISI 420 stainless steel powder on 300M steel substrates [J]. Surface and Coatings Technology, 2018, 333: 210-219.
- [6] Rahman Rashid R A, Nazari K A, Barr C, et al. Effect of laser reheat post-treatment on the microstructural characteristics of laser-cladded ultra-high strength steel [J]. Surface and Coatings Technology, 2019, 372: 93-102.
- [7] Liu J, Li J, Cheng X, et al. Effect of dilution and macrosegregation on corrosion resistance of laser clad AerMet100 steel coating on 300M steel substrate [J]. Surface and Coatings Technology, 2017, 325: 352-359.
- [8] Lourenço J M, Sun S D, Sharp K, et al. Fatigue and fracture behavior of laser clad repair of AerMet® 100 ultra-high strength steel [J]. International Journal of Fatigue, 2016, 85: 18-30.
- [9] Sun G F, Yao S, Wang Z D, et al. Microstructure and mechanical properties of HSLA-100 steel repaired by laser metal deposition [J]. Surface and Coatings Technology, 2018, 351: 198-211.
- [10] Rahman Rashid R A, Barr C J, Palanisamy S, et al. Effect of clad orientation on the mechanical properties of laser-clad repaired ultra-high strength 300M steel [J]. Surface and Coatings Technology, 2019, 380: 125090.
- [11] Barr C, Shi D S, Easton M, et al. Influence of macrosegregation on solidification cracking in laser clad ultra-high strength steels [J]. Surface and Coatings Technology, 2018, 340: 126-136.
- [12] Liu J, Li J, Cheng X, et al. Microstructures and tensile properties of laser cladded AerMet100 steel coating on 300M steel [J]. Journal of Materials Science & Technology, 2018, 34(4): 643-652.
- [13] Li Y J, Zou Z D, Chen Z N, et al. Effects of the weld thermal cycle on microstructure and properties of the heat-affected zone of HQ130 steel [J]. Acta Metallurgica Sinica, 1996, 32(5): 532-537.  
李亚江, 邹增大, 陈祝年, 等. 焊接热循环对HQ130钢热影响区组织及性能的影响[J]. 金属学报, 1996, 32(5): 532-537.
- [14] Wang L, Liu Y, Zhou Y, et al. Softening mechanism analysis of welding heat affected zone of low carbon microalloyed steel [J]. Transactions of Materials and Heat Treatment, 2019, 40(4): 106-113.  
王雷, 刘云, 周勇, 等. 低碳微合金钢焊接热影响区软化机制分析[J]. 材料热处理学报, 2019, 40(4): 106-113.
- [15] Li F Q, Feng S, Li M W, et al. Softening phenomenon of heat-affected zone in laser welding of 6082 Al alloys with filler wire [J]. Chinese Journal of Lasers, 2018, 45(11): 1102007.  
李福泉, 冯时, 李明伟, 等. 6082铝合金激光填丝焊热影响区的软化现象[J]. 中国激光, 2018, 45(11): 1102007.
- [16] Li X J, Huang J, Pan H, et al. Microstructure and formability of laser welding joint of QP1180 high-

- strength steel sheet [J]. Chinese Journal of Lasers, 2019, 46(3): 0302006.
- 李学军, 黄坚, 潘华, 等. QP1180 高强钢薄板激光焊接接头的组织与成形性能 [J]. 中国激光, 2019, 46(3): 0302006.
- [17] Jing C N, Fan J C, Ni X M, et al. Microstructure and mechanical properties of laser welded joints for dissimilar steel with different thicknesses [J]. Chinese Journal of Lasers, 2014, 41(8): 0803005.
- 景财年, 范吉超, 倪晓梅, 等. 激光焊接不等厚异种钢接头组织与性能研究 [J]. 中国激光, 2014, 41(8): 0803005.
- [18] Telasang G, Dutta Majumdar J, Padmanabham G, et al. Effect of laser parameters on microstructure and hardness of laser clad and tempered AISI H13 tool steel [J]. Surface and Coatings Technology, 2014, 258: 1108-1118.
- [19] Shie R K, Chen C. Laser transformation hardening of tempered 4340 steel [J]. Metallurgical Transactions A, 1992, 23(1): 163-170.
- [20] Xu B S, Fang J X, Dong S Y, et al. Heat-affected zone microstructure evolution and its effects on mechanical properties for laser cladding FV520B stainless steel [J]. Acta Metallurgica Sinica, 2016, 52(1): 1-9.
- 徐滨士, 方金祥, 董世运, 等. FV520B 不锈钢激光熔覆热影响区组织演变及其对力学性能的影响 [J]. 金属学报, 2016, 52(1): 1-9.
- [21] Li R T, Zuo X R, Hu Y Y, et al. Microstructure and properties of pipeline steel with a ferrite/martensite dual-phase microstructure [J]. Materials Characterization, 2011, 62(8): 801-806.
- [22] Yang L Q, Ding Y X. Status and development of research of laser transformation hardening [J]. Hot Working Technology, 2006, 35(2): 68-70, 74.
- 杨柳青, 丁阳喜. 激光相变硬化技术的研究现状及进展 [J]. 热加工工艺, 2006, 35(2): 68-70, 74.
- [23] Pan F S, Ding P D, Zhou S Z, et al. Effects of silicon additions on the mechanical properties and microstructure of high speed steels [J]. Acta Materialia, 1997, 45(11): 4703-4712.
- [24] Zhou S, Zhang K, Wang Y, et al. High strength-elongation product of Nb-microalloyed low-carbon steel by a novel quenching-partitioning-tempering process [J]. Materials Science and Engineering: A, 2011, 528(27): 8006-8012.
- [25] Son Y I, Lee Y K, Park K T, et al. Ultrafine grained ferrite-martensite dual phase steels fabricated via equal channel angular pressing: microstructure and tensile properties [J]. Acta Materialia, 2005, 53(11): 3125-3134.
- [26] Jacques P J, Furnémont Q, Lani F, et al. Multiscale mechanics of TRIP-assisted multiphase steels: I. Characterization and mechanical testing [J]. Acta Materialia, 2007, 55(11): 3681-3693.
- [27] Shi J, Sun X J, Wang M Q, et al. Enhanced work-hardening behavior and mechanical properties in ultrafine-grained steels with large-fractioned metastable austenite [J]. Scripta Materialia, 2010, 63(8): 815-818.

## Influence of Multilayer Laser Cladding on the Microstructure and Properties of 30CrMnSiNi2A Steel Substrate

Pang Xiaotong<sup>1</sup>, Yao Chengwu<sup>1\*</sup>, Gong Qunfu<sup>2</sup>, Wang Zhijie<sup>2</sup>, Li Zhuguo<sup>1</sup>

<sup>1</sup> Shanghai Key Laboratory of Materials Laser Processing and Modification, School of Materials Science and Engineering, Shanghai Jiao Tong University, Shanghai 200240, China;

<sup>2</sup> PLA 4724 Plant, Shanghai 200436, China

### Abstract

**Objective** Compared with conventional welding repair methods, laser cladding, an advanced surface modification technology, uses nonequilibrium processing conditions, such as rapid heating and cooling, to fabricate similar alloy compositions on the surface of high-strength steel components. The coating can exhibit refined grains and high dislocation density to achieve high strength and ductility of the repair zone. Therefore, it is a potential for the laser repair of high-strength steel surfaces. Traditional welding methods are used to repair high-strength steel using multilayer and multipass repair welding. Multiple welding thermal cycles induce coarse grains in the heat-affected zone (HAZ), which can lead to significant embrittlement and poor impact toughness of the high-strength steel substrate. Similar to traditional welding, the multilayer and multipass thermal cycles in laser cladding can have multiple tempering effects on the substrate hardened zone, which can lead to grain coarsening and strength softening

of the substrate in HAZ. For the multilayer and multipass laser repair of high-strength steel components, in addition to the effective control of the microstructure and performance of the cladding layer, the softening problem of HAZ in the high-strength substrate and the deterioration of mechanical properties (i.e., low strength and poor elongation) must be overcome. Therefore, in this study, the variation trends of the microstructure evolution and mechanical properties of HAZ in the 30CrMnSiNi2A substrate were shown to be beneficial in controlling the strength and ductility of the repaired high-strength steel parts.

**Methods** Multilayer laser cladding 30CrMnSiA powders were processed on thick 30CrMnSiNi2A steel plates with geometric sizes of 120 mm × 60 mm × 10 mm using the 8-kW semiconductor laser (Laserline LDF-8000-60). The laser cladding parameters were as follows: 2100-W laser power, 7.3-mm beam diameter, 9-mm/s laser scanning speed, 10-g/min powder feed rate, 10-L/min powder feed gas flow, 20-L/min coaxial shielding gas flow, and 0.3-mm single clad layer. The substrates were separately cladded using 1–8 layers, and the samples were retained in the air-cooling state. The microstructure was characterized using the Zeiss-AxioCam MRc5 optical microscope and TESCAN-LYRA3 scanning electron microscope. The microhardness was characterized using the Zwick/Roell ZH $\mu$  Vickers microhardness tester with 0.5-kgf load and 15-s holding time. To investigate the mechanical properties of HAZ subjected to different laser thermal cycles, the cladding coating was cut off, and the hardened layer and tempered zone of the substrate were retained. Tensile and impact samples were prepared using the Zwick/Roell Z100 tensile testing machine and 300 J impact testing machine.

**Results** Owing to rapid laser heating, the first cladding layer did not significantly decompose the residual austenite of the substrate for tempering; however, the following layers had an obvious effect on the residual austenite decomposition, which slightly decreased the sample ductility and impact toughness. With an increase in the number of cladding layers, the ductility of the specimen samples increased, and initial crack and crack growth occurred in the high-temperature tempering zone (HTTZ); however, when the cladding layers did not quench the substrate, initial crack and crack growth occurred in the incomplete quenching zone (IQZ) and HTTZ. Moreover, the uniform plastic deformation decreased, resulting in a significant decrease in the elongation.

**Conclusions and Discussions** Each cladding layer can repetitively quench the substrate during multiple cladding. However, the quenching depth gradually decreased with an increase in the number of cladding layers because the former deposited layers absorbed the heat. IQZ occurred when the thermal cycle could not heat the substrate above the austenitizing temperature and the cladding layer that did not quench the substrate began to produce a tempering effect with an increase in the number of cladding layers. Each cladding layer had the tempering effect on the 30CrMnSiNi2A substrate during the multilayer process. With the increasing number of cladding layers, the residual austenite among the substrate martensite lath bundles first decomposed, the carbides gradually precipitated, and the martensite laths coarsened, becoming wider and blocky until the lath martensite completely transformed into a sorbite microstructure. In terms of the mechanical properties of the substrate in HAZ, the tensile strength gradually decreased and the impact toughness gradually increased with the number of cladding layers. Owing to rapid laser heating, the first cladding layer will not decompose the tempered retained austenite (RA) in the substrate; however, the double cladding layers will significantly decompose RA. Because of the decrease in the ductile RA phases, the tensile elongation and impact toughness of the double cladding layers were slightly reduced.

**Key words** laser technique; laser cladding; thermal cycle; heat-affected zone; microstructure; mechanical properties

**OCIS codes** 140.3390; 160.3380; 160.3900